3-D WAVE PROPAGATION IN CYLINDRICAL SINGLE CRYSTAL SOLID-LIQUID BODIES

Yichi Lu and Haydn N. G. Wadley
Intelligent Processing of Materials Laboratory
School of Engineering and Applied Science
University of Virginia
Charlottesville, VA 22903

INTRODUCTION

The large difference in the ultrasonic velocity between the solid and the liquid phases of most semiconducting materials results in reflection/refraction of ultrasound at solid-liquid interfaces and an interest in using laser ultrasonics for sensing solid-liquid interfaces during single crystal growth. Using a ray tracing analysis, a set of measured ultrasonic time of flight (TOF) projection data can yield the ray paths connecting the source to the receiver, which can subsequently be used to reconstruct the solid-liquid interface. In previous work [1] 2-D wave propagation in cylindrical single crystal solid-liquid bodies was used to explore the feasibility of using ultrasound to characterize solid-liquid interfaces during vertical Bridgman growth of semiconductor materials. Detailed study of ray paths, wavefronts and TOF for ultrasound propagating in both transverse and diametral planes of liquid-solid single crystal (Ge) bodies was reported. Numerical simulations indicated that the magnitude and direction of the group velocity, the solid:liquid velocity ratio and the curvature of the interface together controlled the ray bending behavior and thus determined the ultrasonic data across the interface. Knowledge of ray paths at the interface enabled reconstruction of the interface using a small set of ultrasonic TOF's.

The predicted ultrasonic TOF characteristics of 2-D ultrasonic rays propagating through convex and concave solid-liquid interfaces have recently been confirmed by laser ultrasonic experiments conducted on a benchtop model consisting of a liquid (water/ mercury) and a PMMA cylinder, with one end of the PMMA cylinder being machined into either a convex or a concave shape [2]. The experimental work also indicated that the interface curvature can indeed be reconstructed from the measured TOF data using a nonlinear least squares algorithm. To determine optimal interface sensing configurations and to provide guidance for laser ultrasonic sensing of vertical Bridgman growth of single crystal

Review of Progress in Quantitative Nondestructive Evaluation, Vol 16
Edited by D.O. Thompson and D.E. Chimenti, Plenum Press, New York, 1997

semiconductor materials, we extend the 2-D wave propagation analysis to 3-D, and investigate wave propagation in anisotropic cylindrical single crystal solid-liquid bodies where the receiver is located at arbitrary positions relative to the source.

RAY PATH ANALYSIS

Consider a crystal cylinder of radius R, Fig. 1. The axis of the cylinder is chosen to coincide to the x_3 axis. Following Shah [3] the outer boundary of the cylinder is expressed as:

$$\phi_c = \boldsymbol{x}^T \boldsymbol{A}_c \boldsymbol{x} - c_c = 0 \tag{1}$$

where $\mathbf{x} = (x_1, x_2, x_3)$,

$$\boldsymbol{A}_c = \begin{bmatrix} 1 & 0 & 0 \\ 0 & 1 & 0 \\ 0 & 0 & 0 \end{bmatrix} \qquad c_c = R^2 \tag{2}$$

We assume the solid-liquid interface is spherical with a radius, R_c, centered on the x_3 axis. The interface, ϕ_s, can be expressed as:

$$\phi_s = \boldsymbol{x}^T \boldsymbol{A}_s \boldsymbol{x} + \boldsymbol{B}_s^T \boldsymbol{x} + c_s = 0 \tag{3}$$

where

$$\boldsymbol{A}_s = \begin{bmatrix} 1 & 0 & 0 \\ 0 & 1 & 0 \\ 0 & 0 & 1 \end{bmatrix} \tag{4}$$

For convex interfaces,

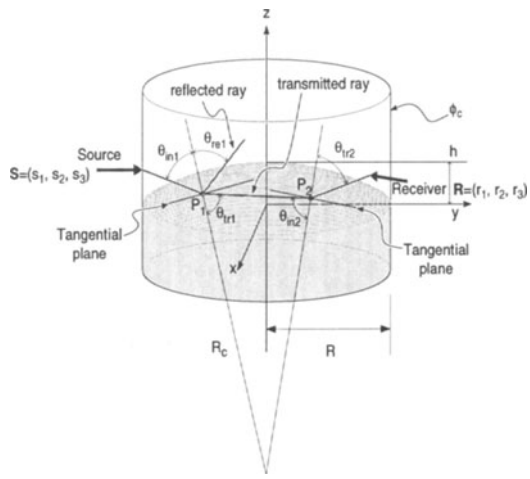

Figure 1. An illustration of 3-D ray tracing in a single crystal solid-liquid body.

$$\boldsymbol{B}_s = \begin{bmatrix} 0 \\ 0 \\ 2(R_c - h) \end{bmatrix} \qquad c_s = h^2 - 2R_c h \qquad h > 0 \tag{5}$$

For concave interfaces

$$\boldsymbol{B}_s = \begin{bmatrix} 0 \\ 0 \\ -2(R_c + h) \end{bmatrix} \qquad c_s = h^2 + 2R_c h \qquad h < 0 \tag{6}$$

In (5) and (6) h defines the interface convexity. The interface is flat when h = 0 ($c_s = 0$). Using R and h, the interface radius R_c can be expressed as:

$$R_c = \frac{R^2 + h^2}{2h} \tag{7}$$

Let **S** be a prescribed source point, $\boldsymbol{l}$ the initial ray direction vector pointing from the source point, **S**. $\mathbf{P}_1$ and $\mathbf{P}_2$ are the first and the second intersection points of the ray path with the interface surface. **R** is the receiver point, while $\boldsymbol{t}_1$ and $\boldsymbol{r}_1$ are the transmitted and reflected ray direction vectors at $\mathbf{P}_1$, $\boldsymbol{t}_2$ is the transmitted ray direction vector at $\mathbf{P}_2$. Thus,

$$\boldsymbol{P}_1 = \boldsymbol{S} + L_1 \boldsymbol{l} \tag{8}$$

where L_1 is the distance from **S** to $\mathbf{P}_1$.

Since $\mathbf{P}_1$ is on the interface it satisfies Eq. (3):

$$\boldsymbol{P}_1^T \boldsymbol{A}_s \boldsymbol{P}_1 + \boldsymbol{B}_s^T \boldsymbol{P}_1 + c_s = 0 \tag{9}$$

Substituting Eq. (8) into Eq. (9) yields

$$L_1^2(\boldsymbol{l}^T \boldsymbol{A}_s \boldsymbol{l}) + L_1(2\boldsymbol{S}^T \boldsymbol{A}_s \boldsymbol{l} + \boldsymbol{B}_s^T \boldsymbol{l}) + (\boldsymbol{S}^T \boldsymbol{A}_s \boldsymbol{S} + \boldsymbol{B}_s^T \boldsymbol{S} + c_s) = 0 \tag{10}$$

Equation (10) yields two roots for L_1. When both roots are complex the ray path does not intersect the interface; when both roots are real and positive the smaller one is the correct solution for L_1; when one root is positive and another is negative, the positive one is the solution for L_1 (the negative root is for the ray travelling in the opposite direction with respect to $\boldsymbol{l}$); when both roots are real and negative, then the ray travels away from the interface (it does not intersect the interface).

The normal $\mathbf{N}_1 = (n_1, n_2, n_3)$ at $\mathbf{P}_1$ to the interface can be obtained using the gradient of the interface:

$$\boldsymbol{N}_1 = \frac{\nabla \phi_s}{\sqrt{(\nabla \phi_s)^T (\nabla \phi_s)}} \tag{11}$$

where

$$\nabla \phi_s = 2\boldsymbol{A}_s \boldsymbol{P}_1 + \boldsymbol{B}_s \tag{12}$$

is the interface gradient at $\mathbf{P}_1$. $\mathbf{N}_1$ is chosen such that it always points into the liquid ($n_3 > 0$).

The incident angle α_{in1} at $\mathbf{P}_1$ to the interface can then be expressed as:

$$\cos\alpha_{in1} = -\boldsymbol{l} \cdot \boldsymbol{N}_1 \tag{13}$$

To determine the reflected and transmitted ray paths, we notice that when a ray is incident upon an interface, both the reflected and transmitted rays propagate in the plane defined by the incident vector, $\boldsymbol{l}$, and the normal to the interface, $\mathbf{N}_1$, at the intersection point $\mathbf{P}_1$ [4 - 9]. If $\mathbf{r}$ is an arbitrary vector in this plane then this plane is given as:

$$(\boldsymbol{r} - \boldsymbol{P}_1) \cdot (\boldsymbol{l} \times \boldsymbol{N}_1) = 0 \tag{14}$$

where $(\boldsymbol{l}\times\mathbf{N}_1)$ is the normal to the plane at $\mathbf{P}_1$.

To determine the reflected and transmitted ray paths at $\mathbf{P}_1$, we need to determine the expression of the stiffness tensor in the plane defined by Eq. (14). We introduce a local coordinate system (x'_1, x'_2, x'_3) in which the x'_2 axis is in the $\mathbf{N}_1$ direction, the x'_3 axis is in the $(\boldsymbol{l}\times\mathbf{N}_1)$ direction, and the x'_1 axis is in the direction defined by $[\mathbf{N}_1\times(\boldsymbol{l}\times\mathbf{N}_1)]$ which is tangential to the interface. Using the directional cosines between (x_1, x_2, x_3) and (x'_1, x'_2, x'_3) the expression of the stiffness tensor in the local (x'_1, x'_2, x'_3) coordinate system can now be obtained following the procedure described by Auld [1, 6]. Knowing the plane in which the incident, reflected, and transmitted rays propagate and the expression of the elastic stiffness tensor in the local (x'_1, x'_2, x'_3) coordinate system, the problem of determining the reflected and transmitted ray paths becomes 2-D and can be solved using the procedures described in a previous publication [1].

For a convex interface and a source point above the interface, a transmitted ray path may intersect the interface again at $\mathbf{P}_2$; the point $\mathbf{P}_2$ is obtained in exactly the same way as $\mathbf{P}_1$. We call this type of ray a doubly transmitted ray. Because $v_s < v_l$, the refraction angle in the liquid is smaller, and there is only one intersection point on the solid-liquid interface for a convex interface when the source point is below the interface or when the interface is concave. This type of ray is called a singly transmitted ray. Using $\boldsymbol{t}_1$ and $\boldsymbol{r}_1$, the second intersection point $\mathbf{P}_2$ and the reflected ray point $\mathbf{R}$ leaving $\mathbf{P}_1$ can be written

$$\boldsymbol{P}_2 = \boldsymbol{P}_1 + L_2\boldsymbol{t}_1, \qquad \boldsymbol{R} = \boldsymbol{P}_1 + L_R\boldsymbol{r}_1 \tag{15}$$

where L_2 is the distance from $\mathbf{P}_1$ to $\mathbf{P}_2$, L_R is the length of the reflected ray leaving from $\mathbf{P}_1$.

All rays eventually intersect the cylinder at $\mathbf{P}_3$. The distance between $\mathbf{P}_2$ and $\mathbf{P}_3$ when there is a second intersection point on the solid-liquid interface, or between $\mathbf{P}_1$ and $\mathbf{P}_3$ when there is only a single intersection point can be determined using Eq. (1). The reflected ray path is then given by $\mathbf{S}$, $\mathbf{P}_1$ and $\mathbf{R}$, the singly transmitted ray path by $\mathbf{S}$, $\mathbf{P}_1$, $\mathbf{P}_3$, while the doubly transmitted ray path is given by $\mathbf{S}$, $\mathbf{P}_1$, $\mathbf{P}_2$, and $\mathbf{P}_3$.

To numerically simulate wave propagation we use the material constants for Germanium (Ge) because its elastic constants as functions of temperature were available for both the solid and the liquid. The analysis can be extended to any anisotropic materials (cubic or non cubic) with know elastic properties. We use the values of elastic constants of Ge at 900°C [10]:

$$c_{11} = 108.45GPa, \qquad c_{12} = 108.45GPa, \qquad c_{44} = 108.45GPa \tag{16}$$

At this temperature the density of the solid $\rho = 5.26$ g/cm^3 [11]. The sound velocity in the liquid (at a temperature just over Ge's melting temperature of 937°C) is 2.71 mm/μs [12]. In all cases R = 37.5 mm.

For a convex interface shape, h = 15 mm, with the source point being located at (0, -R, 15), Figs. 2a and 2b show reflected and doubly transmitted ray paths. When the initial ray directions $\boldsymbol{l}$ are in the diametral plane all ray paths stay in the same plane, since the interface is symmetric with respect to the plane and the normal to the interface at the intersection is also in this plane. When the initial ray directions are not in the diametral plane the reflected and transmitted rays travel away from the diametral plane. Notice most forward propagating doubly transmitted ray paths travel in the diametral plane; the doubly transmitted rays that do not travel in the diametral plane propagate backward due to severe ray bending. Figs. 3a and 3b show reflected and singly transmitted ray paths for a concave interface shape, h = -15 mm, with the source point being located at (0, -R, 15 mm). No doubly transmitted ray paths exist for this case.

When the initial ray directions are in the diametral plane and the interface curvature is symmetric with respect to this plane, rays always travel in the diametral plane. Thus, the plane in which reflected and refracted rays travel is known *a priori*. When the initial ray

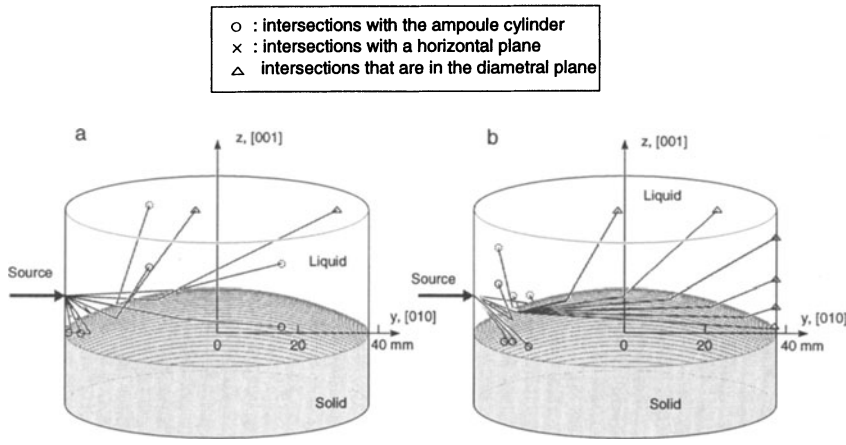

Figure 2. Ray paths for a convex interface, h = 15 mm, s_3 = 15 mm. (a) reflected ray paths; (b) doubly transmitted ray paths.

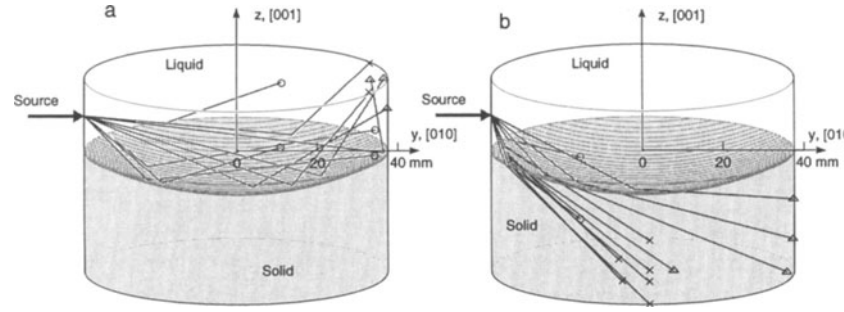

Figure 3. Ray paths for a concave interface, h = 15 mm, s_3 = 15 mm. (a) reflected ray paths; (b) singly transmitted ray paths.

directions are not in the diametral plane, the plane in which reflected and refracted rays travel is not known beforehand and needs to be determined in order to obtain the reflected and transmitted ray paths. The orientation of this plane *depends upon* the interface curvature and the incident ray direction. More rays travel in the diametral plane than in other planes that can be used for the interface sensing purpose. Thus for ultrasonic characterization of the solid-liquid interface using measured ultrasonic TOF data, positioning the ultrasonic source and receiver in the diametral plane should always be the first choice. There are no fundamental difficulties to using ray paths in non diametral planes for interface sensing, it is just more complex, time consuming, and, possibly less accurate.

SIMULATED TIME OF FLIGHT PROJECTION DATA

Ultrasonic TOF projection data are affected by the crystal orientation, liquid and the solid velocities as well as the interface curvature. To use ultrasonic TOF data for interface sensing, we are interested in ray paths that intersect the solid-liquid interface and thus carry information about the interface. We first examine TOF projection data for a convex interface, h = 15 mm, when the source is above the interface, s_3 = 15 mm. Fig. 4a shows diametral TOF projection data for reflected, singly and doubly transmitted ray paths where the receiver position is translated up and down in the diametral plane. The TOF of reflected ray paths increases with r_3 due to the longer propagation distance, the TOF of the doubly transmitted ray paths coincides with that of the singly transmitted ray paths at $r_3 = 0$, which is the minimum of the projection data. Fig. 4b shows circumferential TOF projection data of reflected and singly transmitted ray paths as functions of receiver angle α as defined in Fig. 4 of ref. 1 for several different vertical receiver positions, r_3. When the source point is above the interface most forwardly propagating doubly transmitted rays travel in the diametral plane, Fig. 2b, a circumferential scan of the receiver point around the ampoule cylinder is unlikely to detect doubly transmitted signals except near the diametral plane. The circumferential TOF values of the reflected ray paths increase with increasing r_3 and decreasing $|\alpha|$ due to the longer propagation distance. The same explanation also applies to the singly transmitted rays. Due to the screen effect of the interface, only doubly transmitted rays exist near the diametral plane in the region $0 < r_3 < 15$ mm.

Fig. 5a and 5b show diametral and circumferential TOF data for a convex interface where the source is below the interface at (0, -R, -15). In the diametral plane the TOF of the direct rays has a maximum at r_3 = -15 mm where the solid velocity is minimum. The TOF of transmitted rays increases with the receiver position due to longer traveling distance. The behavior of circumferential TOF is relatively simple, the higher the receiver position, the greater the TOF value. Figs. 6a and 6b show TOF for a concave interface, h = -15 mm, where the source point is above the interface at (0, -R, 15). There is a null in the diametral plane between -15 mm $< x_3 <$ 15 mm. The circumferential TOF data for the reflected rays has large values when $|\alpha|$ is small due to the longer propagation distance. The transmitted rays are either concentrated near the diametral plane or travel way below the interface, Fig. 3b, they are not shown in Fig. 6b.

An inspection of TOF projection data reveals that both the values and the shape of TOF curves are different for different sensing configurations and interface curvature. For instance, concave interfaces are characterized by a steep hump in circumferential TOF curves near $\alpha = 0°$. For the convex interface when the source point is above the interface, singly transmitted rays can be detected circumferentially near the interface, while for the concave interface, the singly transmitted rays travel down into the solid cylinder, Fig. 3b, except those in the diametral plane. Thus, measurable TOF data for singly transmitted rays

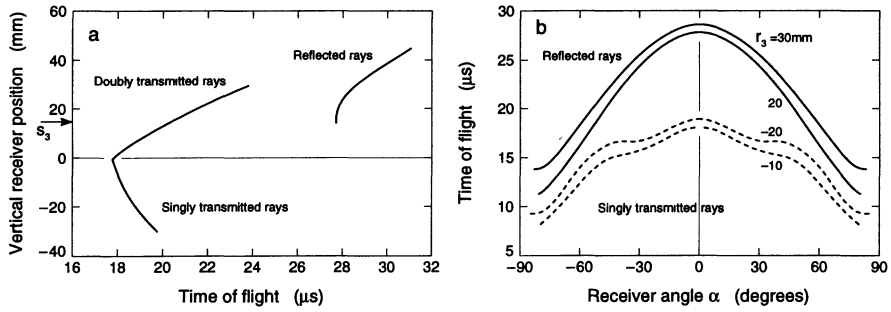

Figure 4. A convex interface, h = 15 mm, s_3 = 15 mm. (a) Diametral TOF data as a functions of the vertical receiver coordinate; (b) circumferential TOF data as functions of the receiver angle.

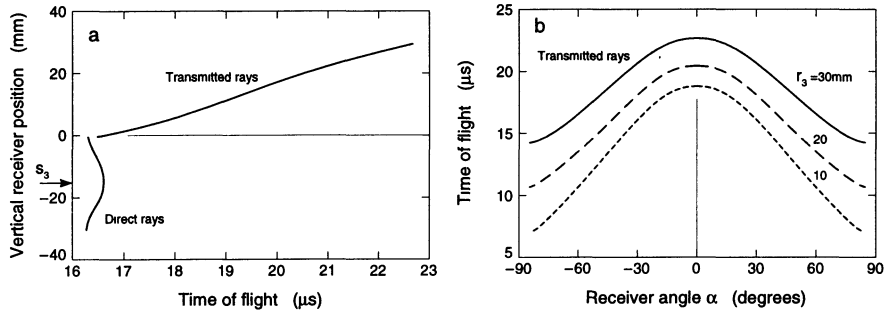

Figure 5. A convex interface, h = 15 mm, s_3 = -15 mm. (a) Diametral TOF data as a functions of the vertical receiver coordinate; (b) circumferential TOF data as functions of the receiver angle.

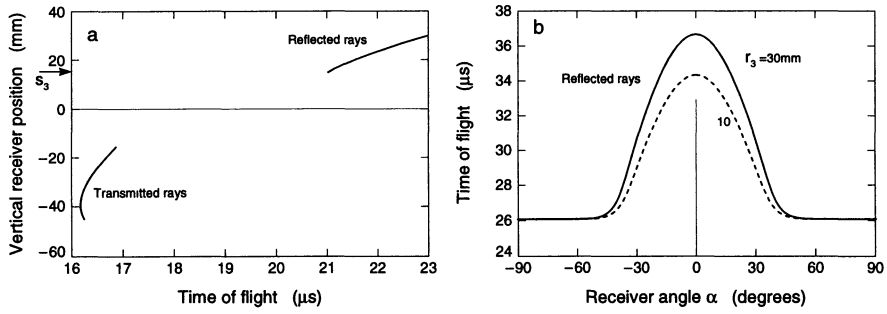

Figure 6. A concave interface, h = -15 mm, s_3 = 15 mm. (a) Diametral TOF data as a functions of the vertical receiver coordinate; (b) circumferential reflected TOF data as functions of the receiver angle.

near an interface would indicate a convex interface shape. On the diametral plane determining whether the convex interface is above or below the source point can be easily done by inspecting the TOF curves, Figs. 4a and 5a. For concave interfaces, the TOF values for rays that travel below the interface when the source point is above the interface (transmitted rays) are much larger that those when the source point is below the interface (direct rays, not shown), while the TOF values for rays that travel above the interface when the source point is above the interface (reflected rays) are much smaller that those when the source point is below the interface (transmitted rays, not shown). If we compare Figs. 4a and 6a where $s_3 > 0$, we find that for a convex interface the TOF of transmitted rays increases with decreasing r_3, while for a concave interface the TOF of transmitted rays decreases with decreasing r_3.

CONCLUSIONS

Three-dimensional ray path, wavefront, and TOF simulations have been conducted in a cylindrical single-crystal solid-liquid bodies. It has been demonstrated that positioning sensors near the diametral plane is the most promising sensing configuration for solid-liquid interface sensing because: (1) the plane in which reflected and transmitted rays propagate is known, and (2) more ray paths with different properties (reflected, transmitted) are available in this plane for interface reconstruction purpose. There is no fundamental difficulty to use ray paths in non diametral planes, it is just more complicated to use them and fewer rays are available for interface reconstruction. The TOF projection data for different sensing configurations and different interface curvature are distinctively different, indicating the promising potential of laser ultrasonic sensors for solid-liquid interface determination during single crystal growth.

ACKNOWLEDGMENTS

This work has been performed as a part of the research of the Infrared Materials Producibility Program conducted by a consortium that includes Johnson Matthey Electronics, Texas Instruments, II-VI Inc., Loral. the University of Minnesota, and the University of Virginia. We are grateful for the many helpful discussions with our colleagues in these organizations. The consortium work has been supported by ARPA/CMO under contract MD A972-91-C-0046 monitored by Raymond Balcerak.

REFERENCES

1. Yichi Lu and Haydn. N. G. Wadley, J. Acoust. Soc. Am., 98, 2663, (1995).
2. D. T. Queheillalt, Y. Lu, and H. N. G. Wadley, J. Acoust. Soc. Am., (submitted, 1996).
3. Pravin M. Shah, Geophysics, 38, 600, (1973).
4. F. I. Fedorov, *Theory of Elastic Waves in Crystals*, (Plenum Press, New York, 1968).
5. M. J. P. Musgrave, *Crystal Acoustics*, (Holden-Day, San Francisco, 1970).
6. B. A. Auld, *Acoustic Fields and Waves in Solids*, (Krieger, Malabar, Florida, 1990).
7. E. G. Henneke, J. Acoust. Soc. Am. 51, 210, (1971).
8. A. Atalar, J. Acoust. Soc. Am. 73, 435, (1983).
9. S. I. Rokhlin, T. K. Bolland, and L. Adler, J. Acoust. Soc. Am., 79, 906, (1986).
10. Yu. A. Burenkov and S. P. Nikanorov, Soviet Physics-Solid State, 12, 1940, (1971).
11. V. M. Glasov, S. N. Chizhevskaya, and N. N. Glagoleva, *Liquid Semiconductors*, (Plenum, New York, 1969).
12. V. M. Glazov, A. A. Aivazov, and V. I. Timoshenko, Soviet Physics-Solid State, 18, 684, (1976).